JTTEE5 17:234–243
DOI: 10.1007/s11666-008-9164-6
1059-9630/$19.00 © ASM International

Development and the Implementation of High-Temperature Reliable Heaters in Plasma Spray Technology

Maria Prudenziati

(Submitted April 26, 2007; in revised form August 9, 2007)

Many problems have been encountered during development of reliable high-temperature heaters by means of atmospheric plasma spray and procedures commonly adopted in thermal spray technology, especially due to poor steel substrate corrosion resistance, notably affected by grit-blasting operations, but also deriving from contamination of insulating layers, dielectric arcs, and failures due to hot spots in the heating elements. While seeking the origin of these problems, a close scrutiny of every single step of the preparation process and analyses of the coatings were carried out using laser confocal scanning microscopy, optical and electronic microscopy, fluorescence analysis, X-ray diffraction, and ancillary techniques. The electrical properties of both alumina layers and metal strips prepared with Ni, NiCr, NiAl commercial powders for the heating elements were studied and cross-related to the failures in the heaters. The article reports the main results of these investigations, delineates the innovations introduced to overcome or circumvent the problems, and underlines the distinct characteristics of new heaters, whose reliability has been proven up to now with temperatures of up to 600 °C in air.

Keywords atmospheric plasma spray, heaters, high temperature operation, multilayer coatings, reliability, temperature sensors

1. Introduction

Plasma-sprayed materials have been used for decades in a variety of engineering applications, such as aerospace and mechanical systems, manufacturing environments, and biomedical implants. In this additive material process, molten or semi-molten particle droplets are propelled onto a substrate where they impact, spread, solidify rapidly and form an adhered coating deposit. An extremely wide variety of materials can be deposited using this technique. High throughput and the ability to deposit on large complex-shaped surfaces are additional advantages of this technology. In recent decades, studies of plasma spray coatings have evolved from being a semi-empirical approach to a more scientific one, leading to a better understanding of the correlation between spraying conditions and coating properties.

Plasma-sprayed active components and devices are, however, still in their infancy. ''Smart'' coatings prepared with masked spraying techniques for sensors were reported by Fasching et al. (Ref 1) about 10 years ago, while mask-less direct writing techniques for sensors and electronic components are under development (Ref 2).

In this scenario, the development of high-temperature heaters emerges as a model system for demonstrating the capabilities of the plasma technique in implementing reliable multilayered devices for industrial equipments and sensor applications. Thermal-sprayed heaters have been developed for systems operating at relatively low temperatures, e.g., pipelines for hot air and water (Ref 3) or copying and printing machines (Ref 4). The development of high-temperature heaters, however, proved to be very elusive, being beset by problems and limitations (Ref 5-7). For example, Younis et al. (Ref 5) reported efforts to develop plasma-sprayed resistors either in Ni or Mo, which were affected by large temperature variations over the surface of a given film, occurrence of electric arc, fractures and localized melting of the heater film. Gadow et al. (Ref 7) report on problems experienced with heaters based on Ni20Cr strips for temperatures above 350 °C.

The work described in this article was aimed at developing plasma-sprayed heaters capable of operating over long periods at temperatures as high as 600 °C in air. This goal has been successfully achieved after a close scrutiny of each single step of the process and analysis of each prepared layer aimed at identifying the failure modes which caused those initial fruitless efforts. It was necessary to discontinue procedures commonly used in thermal spray technology, as well as to design new strategies for avoiding oxidation/corrosion effects responsible for corona discharges, deterioration of electrical properties of the sprayed layers, and to preserve the performance of the heaters over long time periods. The problems that emerged and the strategies adopted will be described next.

Maria Prudenziati, Physics Department, University of Modena, Via G.Campi, 213/A, 41100 Modena, Italy. Contact e-mail: Prudenziati.maria@unimo.it.

2. Experimental

2.1 Materials and Methods

The design included planar and cylindrical heaters (hot runners) on steel substrates with heating elements according to criteria presented here, also accounted for in (Ref 8-11). A schematic representation of the heater plate is given in Fig. 1: a blank alumina coating electrically insulates the heating element (a meander) from the substrate while a second alumina near-blank coating, which covers the whole meander except for the two pads for electrical contact, protects the heating element from the environment and provides electrical insulation (Ref 12). Finally, a glassy thick film laid on the second dielectric layer ''seals'' it from moisture and environmental contaminants, while a flash-evaporated gold film minimizes the energy loss due to infrared emission from the hot surface at temperatures higher than 250 °C (Ref 10).

The selection of materials for this structure (and the analogous cylindrical heater) was guided by the following considerations.

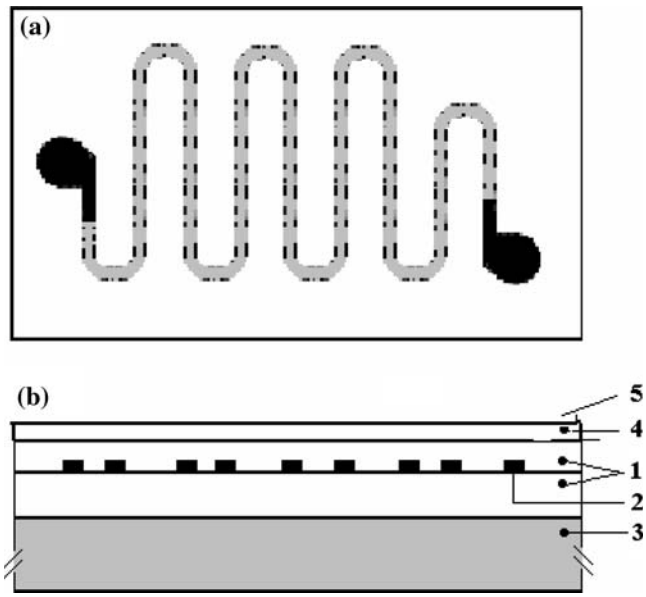

Fig. 1 Heating plate design: (a) plane view and (b) cross section view. The substrate (3) is a metal coupon insulated by a first alumina layer (1) is ~100 μm thick; the conductive meander (2) is 25-30 μm thick, 2 mm wide. The latter is protected by a second alumina layer. The glassy film (4), ~20 μm thick, is covered by a flash evaporated metal film (5)

For economical reasons, as well as to meet the requirements of the intended applications, the substrate cannot be restricted to ''high-quality'' corrosion-resistant alloys (e.g., super-alloys) but rather has to include iron-based alloys such as low carbon steels. The main requirement was a suitable match between the thermal expansion coefficients of the base and its coatings. Table 1 describes the composition of the steels examined and used as substrates in our work. Bronze and aluminum substrates were also used in our investigations for references. In the first stage of development, the substrates were degreased and grit-blasted before the plasma spray process was begun, following to the conventional procedures in thermal spray technology. Both ''white'' alumina, i.e. α-Al_2O_3 (Smyris S.p.A) and alumina-titania (Metcolite, Metco) grits, were used in the blasting operation. A bond coat based on either NiCoCrAlY (Metco 461 NS), Ni20Cr (Amperit 251.1) or Ni5Al (Metco 450 NS) was then sprayed. However, these conventional processes were eventually discontinued because of the related oxidation/corrosion phenomena; hence a proper interface between the substrate and the first alumina coating was attained according to the methods described next.

Plasma-sprayed alumina was deemed to be a suitable material for the electrical insulation of the substrate from the resistive heater (Ref 13, 14) as well as for the top-layer, notwithstanding its intrinsic porosity (Ref 14). Metco 105 SFP and Amperit 740.1 powders (both 99.5 wt.% α-Al_2O_3) were used.

For the resistive heating element, obvious economic and technical considerations restrict the choice to non-precious metals. We investigated the traditional Ni20Cr alloy [(usually selected for its negligible temperature coefficient of resistance (TCR)] as well as Ni (suitable for auto-controlled heaters, due to its high positive TCR values, mainly for low-voltage operating heaters). Ni5Al was also used for comparison. The powders' compositions are listed in Table 2. Metal (either copper or steel) masks were engraved to shape (either a meander or a spiral pattern). Cylindrical masks for heat runners and planar masks for heating plates were cut with a CO_2 laser.

Four different suppliers were asked to prepare the heaters, according to our design. All of them adopted a F4 MB torch and similar deposition parameters. Typical values are reported in Table 3**.** However, comparison of the characteristics if samples deposited by the four suppliers revealed substantially different behavior (Ref 5), in terms of reproducibility, reliability, and life span. Our task was to identify the origin of poor performances, failure modes, and develop remedies to provide reliable heaters.

Table 1 Composition (wt.%) of steels used

Steel	C	Mn	Si	Cr	Ni	P	S	V	Mo
1.2311	0.35	0.80	0.40	1.20	…	…	…	…	0.35
1.2316	0.28	0.95	0.38	14.2	<0.5	0.03	0.03	…	1.1
1.2714	0.55	0.8	0.25	1.1	1.7	…	…	0.10	0.5
AISI 304	0.03 max	2	1.00	18-20	8.5-10.5	0.045	0.03	…	…
AISI 316	0.08	2-3	0.75	18-20	8-11	0.04	0.03	…	2-3

Table 2 Metal powders plasma sprayed for the resistive heating element

Facility	Powder	Nominal composition	Others detected elements
3	Metco 56C-NS	>99.3% Ni	…
1	TAFA 1166F	>99% Ni	…
2	Metco 56F-NS	>99.3% Ni	…
2	Praxair Ni-109	5% Al-Ni balance	…
1	Metco 43C-NS	NiCr	…
4	Amperit 251.1	20Cr-Ni balance	Silicon
3	Metco 43VF-NS	20Cr-Ni balance	…
1	Metco 450 NS	4.5% Al-Ni balance	Silicon

Table 3 Plasma spray deposition parameters for insulator and resistor

Deposition parameters	Al_2O_3	Ni resistor
Deposition temperature, °C	140	140
Standoff distance, mm	105	110
Nozzle diameter, mm	6	6
Cooling gas: type/pressure, bar	Ar/8.5	Ar/8.5
Plasma gas 1: type/flow rate, Sl/min	Ar/45	Ar/55
Plasma gas 2: type/flow rate, Sl/min	H_2/15	H_2/14
Plasma current, A	520	570
Plasma voltage, V	74	75
Powder feed: carrier gas type/flow rate, Sl/min	Ar/3.5	Ar/2.8

2.2 Measuring and Analytical Methods

The topography of the grit-blasted substrates and coatings was imaged with a laser scanning confocal microscopy (LSCM) Leica TCS SP2 DM IRE2. In order to gather almost immediate, though qualitative, information on the corrosion resistance of the blasted coupons and sprayed samples, accelerated corrosion tests were performed, instead of standard salt spray (FOG) tests (Ref 15). Drops of a saturated solution of NaCl in pure water were placed over the surface of both substrates and layers. This test was effective in the comparative evaluation of both as-received steel coupons having different compositions and of coupons of the same composition before and after sand blasting.

For the study of the phase composition of powders and coatings, X-ray powder diffraction patterns (XRPD) were collected using a Panalytical θ/θ diffractometer. The morphology and microstructure of samples were examined by optical and scanning electron microscopy (SEM) in a Philips XL-40 microscope equipped with a detector for secondary electrons (SED images) and a detector for back-scattered electrons (BSD images). Energy-dispersive X-ray spectroscopy (EDS) analyses were performed using the same instrument. For SEM inspection of their internal microstructure and compositional analyses, samples were cut from transverse sections, mounted in resin, prepared by standard metallographic procedures, and ultrasonically cleaned in acetone for 20 min.

The thickness of the alumina coatings was measured by means of a calibrated coating thickness gauge (Elcometer 345). At least 12 points on each sample were inspected to check homogeneity. The volume resistivity and surface resistance of the alumina coatings were measured according to the electrical configurations (guarded electrodes) and measuring conditions described in ASTM D257 (Ref 16). A DC puncture test apparatus with a spherical upper electrode (10 mm curvature radius) and a bottom electrode consisting of a disk (Φ = 30 mm diameter) was used to evaluate the discharge voltages of alumina coatings, according to the ASTM standard D 3755 (Ref 12). Ten points on each coating were tested with the Fluke 1550B MegaOhmMeter, which supplies a voltage ramp (100 V/s) up to the flashover. The values reported in Sect. 3.2 represent the arithmetic mean and the standard deviation of the multiple tested points. The temperature distribution on the heater surface was evaluated with a thermographic camera (AVIO Model TVS 620).

Fig. 2 Stains on the first alumina layer sprayed on sand-blasted nozzle left at room temperature in humid environment

3. Results

3.1 Substrate Preparation

Figure 2 shows the first alumina layer sprayed on a grit-blasted steel cylinder and merely left in a humid atmosphere after the spray process: the surface is decorated with a myriad of small orange-red stains which after EDS analyses were found to be rich in Fe. The stains are naturally assigned to iron oxides formed, during the process, at the interface between the steel support and the alumina coating and ''percolated'' through the interconnected pores of the alumina coating up to its surface. Similar stains were observed on the alumina layers prepared on basted steel coupons after the accelerated corrosion tests (Ref 9).

The heavy responsibility of grit-blasting in enhancing the oxidation/corrosion of steel substrates is shown in Fig. 3; the amount of scales observed on grit-blasted coupons is drastically greater than that on as-received coupons, after the same accelerated corrosion test. Qualitatively

similar results have been observed for all materials listed in Table 1. Compressive residual stresses, cold work with formation of new structural defects, and embedded contaminants (see below) are thought to contribute to the enhanced corrosion of blasted iron-bearing substrates. The intrinsic porosity of alumina coatings conspires with the limited oxidation/corrosion resistance of the supports to impair the physicochemical properties of the first dielectric layer. Other important consequences of corrosion and oxidation on the functional properties of the system (e.g., on dielectric strength of the alumina coating and contamination of the metal over-laying layers) were observed and will be discussed below. An intermediate bond-coat (prepared with powders of Ni5Al, Ni20Cr, NiCoCrAlY, or the like) only mitigates, but does not circumvent, the above-mentioned problems.

A considerable amount of grit-fragmented particles embedded in the steel support was observed, taking SEM-BSD images of the blasted substrates. These inclusions, not removed during the ultrasound treatment in acetone, have a negative effect on the adhesion of the coatings (Ref 17). Moreover, they are responsible for an increased thermal impedance which results in the heterogeneous temperature distribution on heating elements. In order to circumvent the above-mentioned problems, electroless Ni plating was applied on the grit-blasted steel surface; this plating, with its uniform and impervious thickness, enabled the whole substrate surface to be covered, including the residual grit particles, and therefore effectively prevented corrosion and oxide formation, while preserving an adequate adhesion of the first alumina coating on the steel supports (Ref 10).

Naturally, for substrates like bronze, copper, or aluminum, these approaches are not vital, in principle, provided that iron is not introduced into the system (coatings or substrate surface), for example due to recycled grit or iron-bearing sprayed materials; an example of this latter circumstance will be shown in Sect. 3.3.

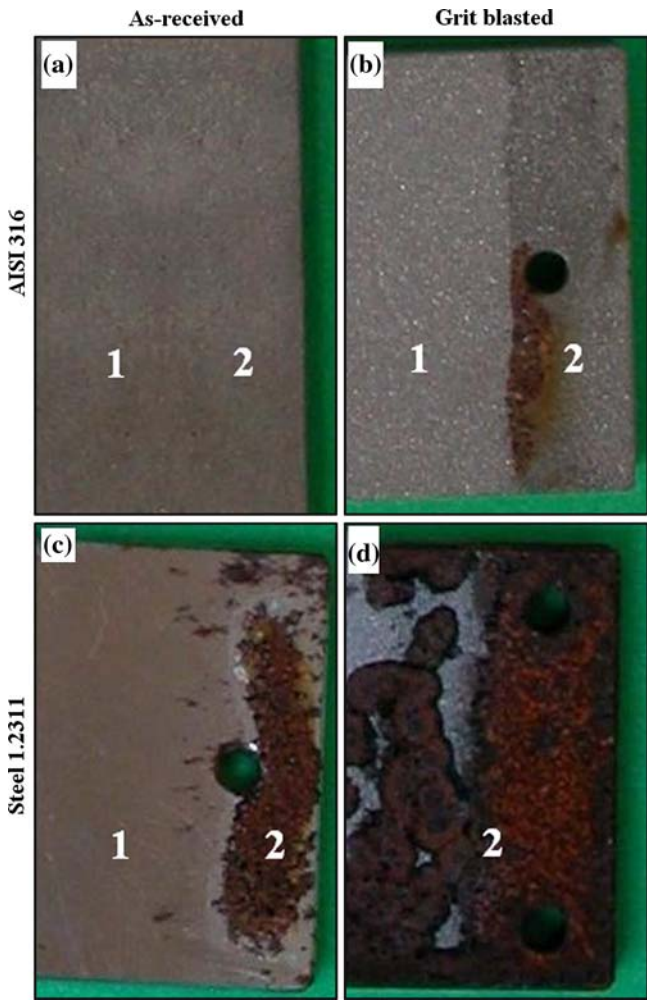

Fig. 3 Results of accelerated corrosion test of as-received (a) and (c) and sand-blasted (b) and (d) steel coupons. Regions marked 1 not dipped in salt solution, regions marked 2 dipped and corroded

3.2 Insulating Layers

Quite different morphologies in terms of porosity, waviness of both the alumina/substrate interface and the alumina top surface were observed for coatings prepared not only by different suppliers but also in various batches from a same supplier.

Table 4 reports typical values of resistivity and surface resistance for the alumina layers. Furthermore, it was found that:

1. The surface resistance is essentially independent of the alumina thickness.
2. The volume resistivity slightly decreases by increasing the coating thickness. The values collected without backing are comparable with those reported by Pawłowski (Ref 18) but lower than those measured recently by Yamasaki and Takeuchi (Ref 19).
3. A backing treatment (120 °C, 12 h) results in a significant increase in the surface resistance but a minor, though not negligible, increase in the volume resistivity. The latter remains, however, more than two orders of magnitude lower than that of sintered (ceramic) α-Al_2O_3, because of the porosity and hydrophilic nature of γ-Al_2O_3 (Ref 20), the main phase in our coatings, as typical for plasma-sprayed Al_2O_3.

Table 4 Surface resistance R_s at 50 V and volume resistivity ρ_v at 500 V for APS alumina coatings

	As-deposited		After backing at 120 °C, 12 h	
Facility/Al_2O_3 thickness	R_s (Ω/sq) × 10^{12}	ρ_v (10^{12} Ω m)	R_s (Ω/sq) × 10^{12}	ρ_v (10^{12} Ω m)
1/80 μm	17.9	0.13	660	2.25
1/156 μm	17.4	0.06	544	1.12
1/207 μm	16.9	0.05	293	0.2
3/150 μm	25	0.04	…	…

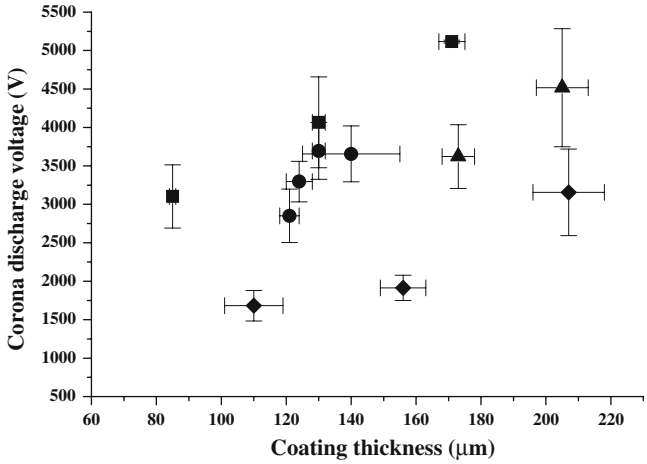

Fig. 4 Corona discharge voltage of alumina as a function of layer thickness for coatings prepared by the facilities: 1, triangles; 2, squares; 3, diamonds; 4, circles. Dots are the average values measured in the first test; bars cover the range of values measured on 10 tested points of the same sample

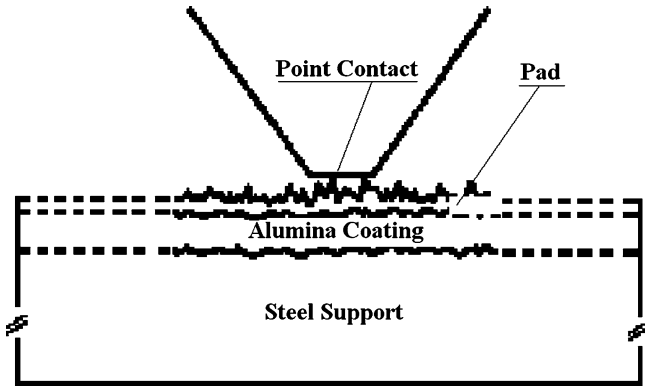

Fig. 5 Metal point contact on a pad

No noticeable difference was found for these properties (surface resistance and volume resistivity) in the study of samples prepared by various suppliers, in contrast to what we observed in experiments of ''dielectric strength''.

Figure 4 shows the voltage values at the onset of the flashover, as a function of alumina coating thickness, measured in samples prepared by various suppliers. The voltage is tagged as ''corona discharge voltage'' in order to underline the real origin of the maximum voltage sustained by the coatings: the ''corona effect'' (Ref 21, 22). As well known this effect does not result in the dielectric breakdown, but it is often accompanied by flashes of light and by slight decreases in volume resistance, which are exactly the phenomena observed in our measurements. Data in Fig. 4 clearly evidences the wide scattering of values around the average for a single sample as well as the extreme differences in performance of samples prepared in various batches. No systematic correlation was found between the discharge values and the sample porosity, differently to other observations (Ref 18, 23). Oxidized/corroded samples exhibited a flashover at voltages several hundred volts lower than those of the parent samples. Further results on this study will be reported elsewhere.

3.3 Heating Elements

The most demanding task in the development of reliable heaters consisted in identifying, and consequently removing, the causes of failures in the heaters during their operation.

The failures all endured the same final catastrophic event; the electrical circuit breaking with discontinuity of the heating element. A variety of different phenomena led to this degradation, including: (i) electric arcs on the pads, (ii) short-circuits through the insulating layer, and (ii) hot spots on the strip or in the region connecting the strip to its pads. The correlation of these phenomena with the sample characteristics is briefly discussed in the following.

Scan profiles of the sprayed metals measured on the meander pads for Ni and Ni20Cr heating elements indicated that the roughness of these surfaces was responsible for a few points of contact with the electrical copper contacts used in the testing set up, consisting in point contacts pressed on the pads (Fig. 5) and therefore created the condition (high spatial concentration of electric field gradients) for electric arcs between the point contacts and the pads. The discontinuity of the electrical contacts was evidenced by the spotted distribution of Cu residues left on the pads by the pressure exercised by the copper contacts themselves (Fig. 6). The more extended contacts introduced for the final devices removed this failure mode (Ref 10).

Short-circuiting through the insulating layer was a distinct failure mode of samples prepared under the following conditions:

1. The use of Ni5Al powders which contained Fe as an impurity.
2. Previous atmospheric plasma spray (APS) processes left unwanted materials in the torch or reservoir for the powders to be sprayed. These materials were included in the sprayed metal strips.
3. In early experiments, when the substrate oxidation was still present (no suitable substrate-alumina interface adopted), iron oxides permeated through the alumina layer and contaminated the resistive strip.

A close selection of the powders, the sequence of processing steps, and the proper substrate-alumina interface ended the occurrence of these short circuits. Hot spots were more intimately related to the nature of the main metal used for the resistive element, its geometric definition, and surface roughness. Examples of this relationship are illustrated in the following.

Figure 7 illustrates results of the analysis performed on a sample which had been damaged on the short leg connecting the pad to the metallic strip of the heater. In this example, the heating element consisted of Ni20Cr and the

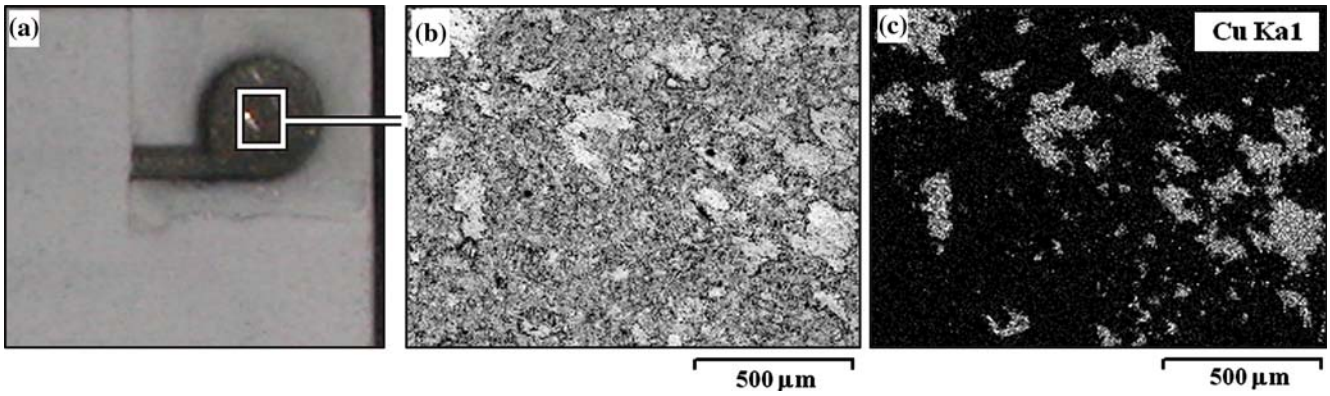

Fig. 6 One pad (a), SEM-SED image (b), and Cu elemental map (c) of the marked area

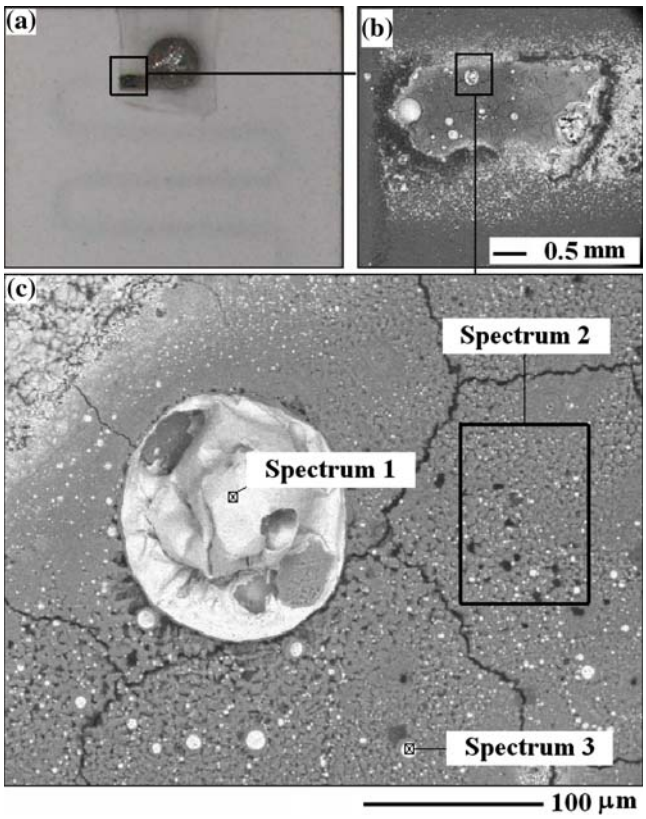

Fig. 7 (a) Position of the damaged area occurred on the short leg connecting the pad to the conductive strip prepared with APS sprayed Ni20Cr powder. (b) Low magnification SEM image of the material affected by the failure. c) BSD-SEM at higher magnification, and marked regions for EDS analyses. For measured composition see Table 5

failure occurred at a mean sample temperature of about 300 °C. The region in which the failure occurred is shown in Fig. 7(a) while SEM images of the damaged area are given in Fig. 7(b) and (c). The composition of various analyzed points and regions is given in Table 5. The most evident feature in the SEM images is the presence of spherules which were found to be oxidized Ni.

Table 5 Concentrations of elements detected with EDS in the region of failure, for the sample described in Fig. 7, where points and region of collected spectra are shown

	Atomic %			
Spectrum	O	Cr	Ni	Al
1	22.6	8.89	68.5	…
2	59.0	5.90	2.05	33.07
3	11.8	6.14	81.1	0.90

The presence of the spherules shows that the melting point T_m of the metal has been exceeded ($T_m = 1453$ °C for Ni and $T_m = 1400$ °C for NiCr). Hence, Cr is ejected into adjacent regions, forming a macroscopically homogeneous phase rich in Al and O. These results show that part of the sprayed strip reacted with the underlying alumina layer. EDS analysis of the cross section of the damaged area provided further evidence of the reaction and allowed us to derive the picture of the transformations that is schematically illustrated in Fig. 8. The same kind of failure mode was observed for heating elements prepared with both sprayed Ni or Ni5Al and at various substrate temperatures from 200 to 500 °C.

A successful remedy for these problems included the preparation of thicker terminations for the stripes (Ref 10). Figure 9 illustrates results of a Ni20Cr-based sample which exhibited a failure on a small point located on the heating element under the protecting alumina layer. Also in this case, the features shown are typical results of many investigated samples. This type of failure first appeared as a hot spot easily observed using the infrared camera but often visible even to the naked eye. A few seconds after its appearance, flashes of intense light were observed, followed by irreversible failure of the heating element. The alumina coating on the spot was altered, having a dark color. Figure 9 shows the position of the analyzed failure in a photo shot (a), its shape as observed by means of optical microscopy (b), and a scanning electron microscopy image (c). The results of the EDS analysis performed in different selected points of the damaged area are given in Table 6. Spectrum 3 shows that oxidized nickel is present in a spherule which is segregated from the other

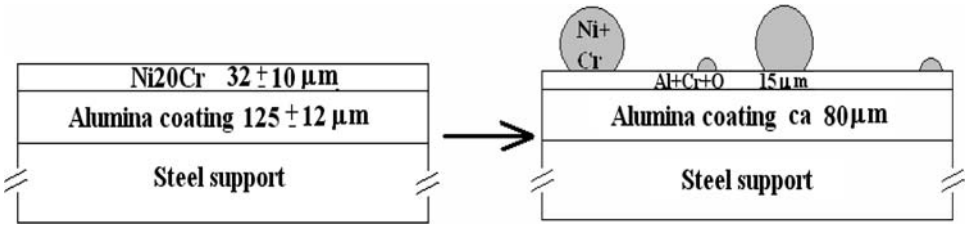

Fig. 8 Schematic representation of the physical and chemical changes occurred on the short leg of the meander near its pad

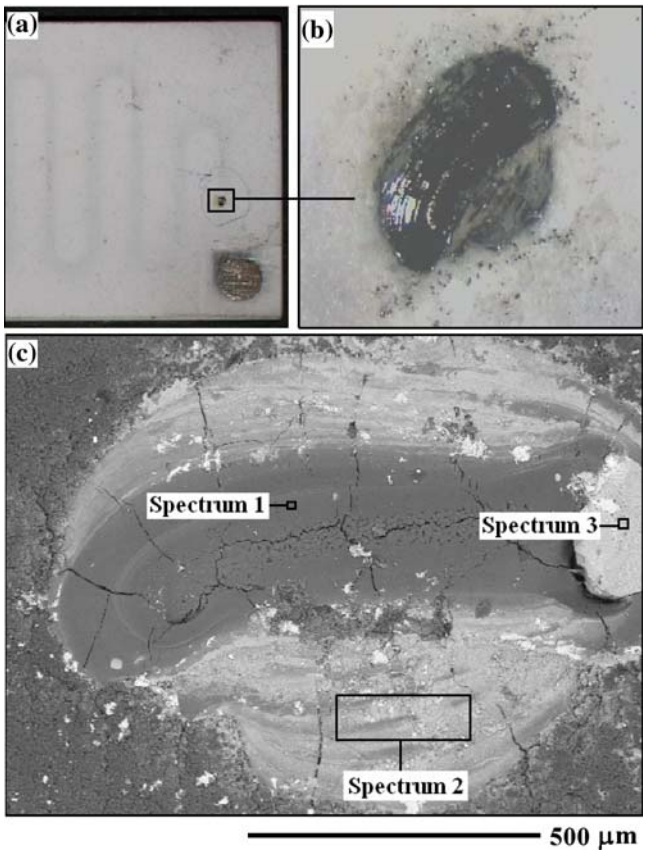

Fig. 9 Heater after an electric spark and failure occurred on a localised point on the metal strip. (a) Part of the sample; (b) optical micrograph of the crater on the strip; and (c) BSD-SEM image and marked regions for EDS analyses. For measured composition see Table 6

metallic elements of the strip. Similar results have been observed in samples with Ni5Al heating elements. In the present case, the outer zones of the ''crater'' consist of an almost homogeneous phase rich in Al and O that includes Cr and Ni. In the middle of the crater an analogous composition was detected but with a different morphology, with presence of dendrites, an effect which suggests a higher local temperature reached by the reacted materials. Details of morphologies varied from sample to sample, as expected, because of the different kinetics of reactions and quenching phenomena accompanying exothermic reactions. However in all the investigated samples exhibiting

Table 6 Concentrations of elements detected with EDS in the region of failure, for the sample described in Fig. 9, where points and region of collected spectra are shown

	Atomic %				
Spectrum	O	Al	Cr	Ni	Fe
1	54.1	36.93	3.28	5.64	…
2	55.51	13.04	5.39	27.25	0.81
3	41.17	0.76	0.86	57.21	…

this type of failure there was the simultaneous presence of Ni, Cr, Al e O in the exposed area. All the mentioned findings suggest that self-propagating reactions, similar to alumino-thermic reactions, are responsible for this type of failure. The observed phenomena are assisted (and their interpretation made harder) by the oxidation and dissociation of feedstock powders during their plasma spraying (Ref 24-26); in fact, our X-ray diffraction analyses of sprayed NiCr often revealed the presence of Cr_2O_3 and chromite ($NiCr_2O_4$), which resulted in heterogeneities of the heating elements.

The defects responsible for the hot spots were identified as:

1. narrowing of a short tract of the heating element which increased the resistance in that region and gave rise to an increased Joule-electrical power and overheating;
2. lifting of the metal strip from the underlying alumina coating, resulting in decreased heat dissipation to the substrate;
3. heterogeneity in the composition of the heating element and presence of impurity phases in the heating element such as Fe (probably an iron oxide), chromium oxide (Cr_2O_3), chromite ($NiCr_2O_4$), and silicon (probably SiO_2).

The resistivity of all of these phases is notoriously higher than that of Ni and its alloys (Ref 27-29). Hence we can argue that they are responsible for a local increase in the electrical resistance and, in turn, for an increase in the dissipated power.

All of these lacks of homogeneity in the electrical properties and the related thermal effects initiate a positive feedback for reactions resulting in a local overheating of the sample. The presence of chromium oxides and chromites was confirmed in diffraction analyses of some

Fig. 10 Optical micrograph of a sample consisting of: bronze as support insulated by alumina (150 μm), Ni20Cr heating trip and alumina top coating. Stains on the metal strip were observed after an accelerated corrosion test and found to be due to iron contamination of the sprayed heating element

coatings of Ni20Cr, while the presence of contamination by Fe, Si, and Cr was a frequent finding in coatings prepared with Ni5Al powders. For instance, contamination of iron in a Ni5Al strip prepared on an alumina covered bronze support was revealed by the occurrence of brown stains after treatment with saturated salt solution (Fig. 10).

The picture emerging from the present work proved that much more serious failure modes are associated with the use of NiCr- and NiAl-based heating elements than of Ni-based ones. This evidence prompted us to focus our attention on Ni-based heaters. The chance of obtaining high-temperature coefficient of resistance with these metal strips was an additional expected benefit deriving from this choice.

3.4 Heaters

Figure 11 shows two types of heaters successfully implemented on the basis of the described design rules and the revised processes; a runner nozzle for polymer injection molding apparatus as described in the patent publication (Ref 8) and a heating plate on a steel coupon (Ref 10-11). Both heating elements consist of Ni strips about 30 μm thick.

The runner nozzle was realized on steel 1.2714 with a mask for deposition of a spiral 2 mm wide and about 605 mm long, which exhibits a resistance of about 4.2 Ω. Heating plates were prepared on various steels (Table 1) using masks capable of patterning meanders 2 mm wide and 210 mm long, with a resistance of about 1 Ω. The resistivity of the sprayed metal ($\rho \approx 22.5$ μΩ cm at 20 °C) was found to be about a factor of 3-4 times higher than that of its dense counterpart (6.8 μΩ cm). Resistance values were found to be reproducible within ±10%. After annealing at a temperature of higher than 350-400 °C, an

Fig. 11 Two types of heaters successfully implemented: a runner nozzle for polymer injection moulding apparatus as described in the patent publication (Ref 8) and a heating plate

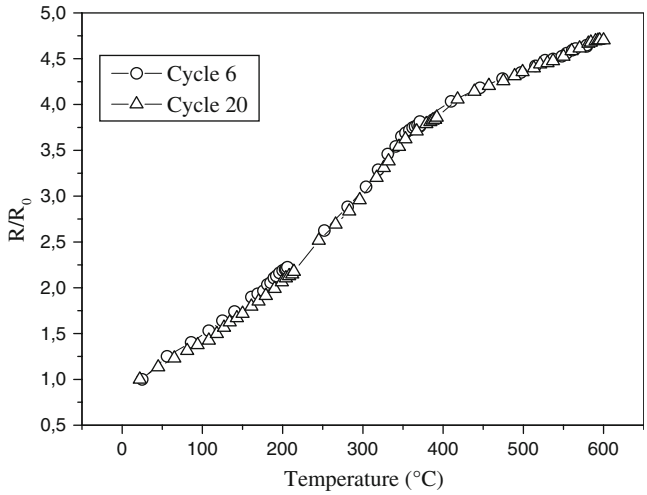

Fig. 12 Resistance versus temperature for the Ni-based heating element. The resistance is normalised to its value at 25 °C. Data are reported for two different thermal cycles

irreversible resistance decrease of about 15% was systematically observed. This finding, together with further data on the electrical properties of sprayed metals, will be described in depth elsewhere.

Figure 12 shows the temperature dependence of the normalized resistance $R(T)/R_0$ with $R_0 = R$ (25 °C). Repeated heating cycles were performed and the behavior was found to be very reproducible. It is remarkable that the R versus T behavior is the same as that expected for plain Ni wires or sheets, with the typical high-temperature coefficient of resistance (TCR) and a notable change in slope at around 400 °C. As is well known, this temperature is close to the Curie point of Ni, where notable changes in magnetic, electrical, and thermal properties occur. The high-temperature coefficient of resistance and the reproducibility and stability of resistance-temperature relationship

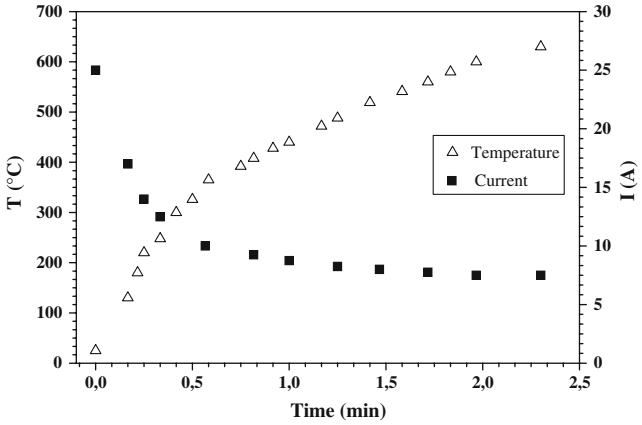

Fig. 13 Temperature versus time for the heating plate shown in Fig. 11, under constant bias voltage of 24.5 V. $R_o = 0.95\ \Omega$

enable an accurate temperature monitoring of the heater without additional temperature sensors.

The fast warm-up of the heating plate is shown in Fig. 13, which displays the temperature as a function of time under a constant bias voltage of 24.5 V. A very fast initial increase in temperature is observed with high current absorption (28 A, ≈690 W), soon followed (in less than a minute) by a slower heating period up to 600 °C.

Thermographic images of the heating plates confirmed a good mean surface temperature distribution, in good agreement with that measured by the thermocouple. However, the strip displays a temperature higher by a few tenths of degree Celsius than the surrounding areas. Emissivity $\varepsilon = 0.95$ of the γ-Al_2O_3 was found, in agreement with the value reported in Ref 30.

This type of heater has been tested for stability of operation throughout repeated heating and cooling cycles, over a time period of about 800 h (500 h at 420 °C plus 50 h at 600 °C). No change in electrical characteristics, structural, and aesthetic features was observed after the tests.

In short, the newly developed heaters exhibit the following distinct characteristics:

- an operating range from room temperature to at least 600 °C. This wide temperature range is uncommon for heaters realized with other technologies. Furthermore, micro-hot plates (Ref 31) and micro-heaters (Ref 32) fail at high temperatures in a short time.
- Fast warm-up.
- Heat transfer at theoretical limit at start up.
- Homogeneity of the temperature distribution over a wide area as a result of the intimate contact between the heating element and the substrate as well as the good thermal properties of the constituents, especially of the substrate.
- Immunity from thermal shock, which notably limits the use of heaters on ceramic substrates.
- Industrial reliability over long time periods at high temperatures.

4. Conclusion

We have reported design criteria and main characteristics of heating elements, prepared with APS processes for industrial applications over a wide temperature range (20-600 °C) and self-regulated. It has been shown that standard (i.e., commonly adopted) processes and commercial materials are responsible for detrimental performance, i.e., limitations or failures, whose origin was identified by a close scrutiny of the failure modes, whereas the related problems were overcome or circumvented by means of the introduction of new strategies. The most rewarding revisions concerned: (i) new procedures enabling us to achieve clean (free from contaminations) interfaces between iron-bearing substrates and their coatings; (ii) selection of simple compositions for the conductive powders; in particular the choice of Ni powders in opposition to NiCr and NiAl powders, since these alloys suffer from detrimental effects such as dissociation, too-strong oxidation, and phase transformations in the plasma plume; and (iii) adequate methods for the electrical tests (e.g., sizeable electrical pressure contacts, instead of point contacts (Ref 10)); sealing of porous γ-alumina coating with a glassy layer (Ref 10, 11).

The results achieved show that atmospheric plasma spraying is also an adequate technology for the production of reliable temperature sensors or self-regulated heating platforms, at least up to 600 °C, for applications in the field of sensors (Ref 33), e.g., heating platforms for high-temperature operating sensors as well as for integration on engineering components and structures (Ref 34). These results are not only interesting per se, but in addition they confirm that ''smart thermally sprayed coatings'' can become a reality, opening up a new dimension for an ''active'' Plasma Spray Technology. This evolution might parallel what occurred in thick-film technology, which started from the manufacture of decorative drawing and evolved to the production of passive components for hybrid microelectronics, as well as for sensors and actuators.

Acknowledgments

The author is indebted to Centro Sviluppo Materiali S.p.A., Roma, Italy (Ing. F. Sintoni, Dr. M.I. Pistelli, Ing. F.Casadei, Mr. E. Severini, and Mr. V. Ferretti), Zocca Officine Meccaniche S.r.l.Funo di Argilato, Bologna, Italy (Ing. G. Dalbagni), Sulzer Metco AG, Wohlen, Switzerland, and Praxair Surface Technologies, Fornovo di Taro, Parma, Italy for the spray coating depositions. Thanks are due to Dr. M. Lassinanti Gualtieri, M.G. Busana, M. Ravarotto, and Dr. V. Volteggiatori for their support in data collection and sample characterization. Ing. Gianfranco Cirri greatly contributed to the project with continuous discussions, criticisms, and precious suggestions. All the analytical work has greatly benefited from the excellent arsenal of equipment available in CIGS (Centro Interdipartimentale Grandi Strumenti) of the University of Modena and Reggio Emilia; the assistance of its staff in the use of XRD, SEM, EDS, and CLSM systems is

gratefully acknowledged. This research has been promoted by INGLASS (formerly INCOS), San Polo di Piave, Treviso, Italy.

References

1. M. Fasching, F.B. Prinz, and L.E. Weiss, Smart Coatings: A Technical Note, *J. Therm. Spray Technol.*, 1995, **4**(2), p 133-136
2. S. Sampath, H. Herman, A. Patel, R. Gambino, R. Greenlaw, and E. Tormey, Thermal Spray Techniques for Fabrication of Meso-electronics and Sensors, *Mater. Res. Soc. Proc.*, 2001, **624** (Materials Development for Direct Write Technologies), p 181-188
3. E. Brook-Levinson, V. Manov, E. Margolin, E. Adar, Y. Sorkine, and V. Volchkov, Electrical Heating Elements and Method for Producing Same, US Patent 6,596,960, July 22, 2003
4. E. Hyllberg Bruce, Ceramic Heater Roller, US Patent 5,616,263, April 1, 1997
5. H.F. Younis, R.S. Dahbura, and J.H. Lienhard V, Thin Film Resistance Heaters for High Heat Flux Jet-array Cooling Experiments, *Proc. ASME Heat Transfer Div.*, ASME HTD, 1997, **353**, p 127-134
6. D. Michels, J. Hadeler, and J.H. Lienhard, V, High Heat Flux Resistance Heaters from VPS and HVOF Thermal Spraying, *Exp. Heat Transfer*, 1998, **11**(4), p 341-359
7. R. Gadow, A. Killinger, and C. Li, Product Development with Thermally Sprayed Functional Coatings on Glass and Glass-ceramics Substrates, *Int. J. Appl. Ceram. Technol.*, 2005, **2**(6), p 493-503
8. G. Cirri and M. Prudenziati, Method for Producing Heated Components for Injection Moulding Apparatus and Heating Equipment in General, US 2005/0257367 A1, November 24, 2005
9. M. Prudenziati, G. Cirri, and P. Dal Bo, Novel High-temperature Reliable Heaters in Plasma Spray Technology, *J. Therm. Spray Technol.*, 2006, **15**(3), p 329-331
10. G. Cirri and M. Prudenziati, Elemento riscaldante innovativo, in particolare per camere calde di apparecchiature di stampaggio ad iniezione di materie plastiche, *Italian Patent Pending* MO2006A000314
11. G. Cirri and M. Prudenziati, Tecnica innovativa per il miglioramento delle caratteristiche dielettriche e di anticorrosione di ricoprimenti ottenuti con tecnologie thermal spray, APS, HVOF e analoghe, in particolare di riporti isolanti quali ad es. Al2O3, *Italian Patent Pending* MO2006A000322
12. ASTM D 3755 Standard Test Method for Dielectric Breakdown Voltage and Dielectric Strength of Solid Electrical Insulating Materials Under Direct-Voltage Stress
13. L. Golonka and L. Pawłowski, Ceramic on Metal Substrates Produced by Plasma Spraying for Thick Film Technology, *Electrocomp. Sci. Technol.*, 1983, **10**(2-3), p 143-150
14. R. McPherson, *Surface Engineering Processes and Applications*, K.N. Strafford, R.St.C. Smart, I. Sare, and C. Subramanian, Eds. (Lancaster), Technomic Publications, 1995, p 3-20
15. ASTM B 117-73 Standard Test Method of Salt Spray (FOG) Testing and ASTM B 117-90 Standard Test Method of Salt Spray (FOG) Testing
16. ASTM D257 Standard Test Methods for DC Resistance or Conductance of Insulating Materials and Volume and Surface Resistivity Measurements of Insulating Materials Using the Model 6517A Electrometer/High Resistance Meter. Application Note Keithley, Series Number 314
17. M. Mellali, A. Grimaud, A.C. Leger, P. Fuchais, and J. Lu, Alumina Grit Blasting Parameters for Surface Preparation in the Plasma Spraying Operation, *J. Therm. Spray Technol.*, 1997, **6**(2), p 217-227
18. L. Pawłowski, The Relationship Between Structure and Dielectric Properties in Plasma-sprayed Alumina Coatings, *Surf. Coat. Technol.*, 1988, **35**(3–4), p 285-298
19. R. Yamasaki and J. Takeuchi, Physical Characteristics of Alumina Coating Using Atmospheric Plasma Spraying (APS) and Low Pressure Plasma Spraying (VPS). Proc. ISTC Spray 2004: Advances in Technology and Application, B.R. Marple and C. Moreau, Eds., Osaka, Japan: DVS Verlag, 2004, p 283-285
20. K. Sohlberg, S.J. Pennycook, and S.T. Pantelides, Hydrogen and the Structure of Transition Aluminas, *J. Am. Chem. Soc.*, 1999, **121**(33), p 7493-7499
21. H.J. Kim, S. Odoul, C.H. Lee, and Y.G. Kweon, The Electrical Insulation Behavior and Sealing Effects of Plasma-sprayed Alumina-Titania Coatings, *Surf. Coat. Technol.*, 2001, **140**(3), p 293-301
22. E. Turunen, T. Varis, S.-P. Hannula, A. Vaidya, A. Kulkarni J. Gutleber, S. Sampath, and H. Herman, On the Role of Particle State and Deposition Procedure on Mechanical, Tribological and Dielectric Response of High Velocity Oxy-Fuel Sprayed Alumina Coatings, *Mater. Sci. Eng. A*, 2006, **415**(1-2), p 1-11
23. E.J. Young, E. Mateeva, J.J. Moore, B. Mishra, and M. Loch, Low Pressure Plasma Spray Coatings, *Thin Solid Films*, 2000, **377-378**, p 788-792
24. K. Volenik, B. Kolman, J. Dubsky, and P. Chraska, In-Flight Behaviour of Ni-Al Powder During its Plasma Spraying. Proceed. ITSC 2005-Thermal Spay Connects: Explore its Surfacing Potential!, E. Lugscheider, Ed., Duesseldorf, Germany: DVS-Verlag GmbH, 2005, p 1175-1178
25. G. Espie, A. Denoirjean, P. Fauchais, J.C. Labbe, J. Dubsky, O. Schneeweiss, and K. Volenik, In-Flight Oxidation of Iron Particles Sprayed Using Gas and Water Stabilized Plasma Torch, *Surf. Coat. Technol.*, 2005, **195**(1), p 17-28
26. P. Chraska, B. Kolman, M. Suchanek, and K. Volenik, Composition Changes of Selected Alloys During Their Plasma Spraying. Proc. ITSC Spray 2004: Thermal Spray Solutions—Advances in Technology and Applications, B.R.. Marple and C. Moreau, Eds., Osaka, Japan: DVS Verlag, 2005, p 7-11
27. R.C. Weast, Eds., Handbook of Chemistry and Physics, (50th ed.). The Chemical Rubber Company CL, Ohio, 1969
28. H. Liu, E.Y. Jiang, R.K. Zheng, and H.L. Bai, Structure and Transport Properties of Polycrystalline Fe_3O_4 Films, *J. Phys. C. Cond. Matter*, 2003, **15**(46), p 8003-8009
29. E.J. Verwey, P.W. Haayman, and F.C. Romeijn, Physical Properties and Cation Arrangement of Oxides with Spinel Structures, II. Electronic Conductivity, *J. Chem. Phys.*, 1947, **15**(4), p 181-187
30. R. Gadow, A. Killinger, and C. Li, Online Process Control of Plasma Sprayed Ceramic Coatings with IR Thermographic Imaging. Proc. ITSC 2002, E. Lugscheider, Ed., Dusseldorf, Germany: DVS-Deutscher Verband für Schweißen, 2002, p 573-579
31. D. Briand , F. Beaudoin, J. Courbat , N.F. de Rooij, R. Desplats, and P. Perdu, *Microelec. Reliab.* 2005, **45**(9-11), p 1786-1789
32. T. Tong, J. Li, Q. Chena, J.P. Longtin, S. Tankiewicz S. Sampath, Ultrafast Laser Micromachining of Thermal Sprayed Coatings for Microheaters: Design, Fabrication and Characterization, *Sens. Actuators A*, 2004, **114**(1), p 102-111
33. E.M. Gualtieri and M. Prudenziati, Sistema per la rivelazione di composti organici tossici pesanti in aria, *Italian Patent Pending* MO2006A000151
34. G. Cirri and M. Prudenziati, Metodi innovativi per la produzione di piani di cottura in ceramica o in vetro con riscaldatore integrato, per cucine domestiche ed autoregolato in temperatura, *Italian Patent Pending* MO2006A000413